RSC Advances

ROYAL SOCIETY
OF CHEMISTRY

www.rsc.org/advances

Cite this: DOI: 10.1039/c0xx00000x

www.rsc.org/xxxxxx

ARTICLE TYPE

A Strong Charge-Transfer Effect in Surface-Enhanced Raman Scattering Induced by Valence Electrons of Actinide Elements

Yang Gao,[a,b] Lei Chen,[a,b,c] Xing Dai,[a,b] Ruixia Song,[a,b] Bo Wang,[a,b] Zhigang Wang*[,a,b]

Received (in XXX, XXX) Xth XXXXXXXXX 20XX, Accepted Xth XXXXXXXXX 20XX

DOI: 10.1039/b000000x

Surface-enhanced Raman scattering (SERS) is a powerful spectroscopic technique for highly sensitive molecular detection. Due to great radial extent of 5f/6d orbitals is enough to support surface plasmons, the SERS substrate materials containing actinide elements might bring a novel enhancement mechanism and even significant enhanced magnitude. Here we study the SERS of a pyridine molecule on the typical actinide embedded structure Ac@Au_7 and on the similar structure of pure gold Au_8, respectively, using the time-dependent density functional theory (TDDFT) method. The calculated results show that the absorption spectrum of pyridine-Ac@Au_7 at 456 nm presents a strong peak belonging to charge-transfer (CT) transition from the metal to the pyridine molecule. Surprisingly, the corresponding CT-SERS enhancement can reach the order of magnitude of 10^5, which could hardly be achieved in the pure gold systems (about $10^3 \sim 10^4$). Furthermore, electronic structure analysis reveals that the initial orbitals of CT transition contain non-ignorable contribution from 6d electrons of the Ac atom. Meanwhile, the contribution of 6d electrons can be tuned by changing the conformation of pyridine-Ac@Au_7 complex. The current findings provide a theoretical basis for exploring and synthesizing SERS materials based on actinide elements, which might subsequently facilitate applications of such structure in nanostructural characterization, single-molecule SERS signal detections and biological molecular recognitions *etc*.

Introduction

It is well known that an appropriate metal substrate is the prerequisite for observing surface-enhanced Raman scattering (SERS), and its composition directly determine the intensity of SERS signals, so how to select their components has been a core issue in analytical technique.[1, 2] In fact, all metals can enhance local electromagnetic field more or less, the intensity of enhancement mainly depend on the ability of metals to support high resonance quality of surface plasmons, *i. e.*, the optical property of substrate materials directly involved with their electron structures.[2] Among them, because the valence shell electrons (...$3d^{10}4s^1$ for copper, ...$4d^{10}5s^1$ for silver, ...$5d^{10}6s^1$ for gold) are very active chemically, coinage metals have been well designed and fabricated as particularly promising SERS substrate materials.[1] Meanwhile, other metal substrate materials have also been widely developed in this field, such as Li, Na, K, Co, Ni, Pt, Rh, Pd *etc*.[2, 3] Obviously, for the above mentioned metals, their isoelectronic shells all contain similar unsaturated electrons which make them obtain great SERS enhancement. Thus, actinide elements would have great advantage in supporting surface plasmons due to their chemically hyperactive valence orbital electrons.

Currently, the SERS experiments have found that the valence electrons (5f,6d) of actinide elements can induce intense charge-transfer (CT) transition between metals and molecules.[4] However, because the optical resonance excitation of the system (containing 5f/6d orbitals) is severely affected by the inherent complexity which might arise from the metal nanoparticles, the probe molecule and the metal-adsorbate system, to get a full understanding of SERS enhancement mechanism remain facing enormous challenge. Therefore, a comprehensive theoretical prediction is essential for further exploration and synthesis of multifunctional SERS substrate materials. In single-molecule SERS (SM-SERS) signal detections, the multicomponent substrates not only can control the optical properties of the metal-molecule complexes, but also can facilitate the selection of excitation lights to match the experimental requirements.[5-13] Furthermore, our reported works have also pointed out the binary coinage metal clusters have great advantages in tuning the excitation light for SERS spectra, compared with the pure element clusters.[12, 13] Moreover, although silver is more plasmonically active than gold in SM-SERS and ultrasensitive SERS experiments, gold is more chemically inert, high biocompatible and hypo-toxic, so gold is preferred in medical applications. This means the chemical stability of substrate materials is also more important than maximum enhancement.[14] With the successful application of a series of heavy elements (Ac, U, Gd),[15-19] the designed mixed-metal of gold-actinides has great applying prospect in biosystem.

Nowadays, the observed huge SERS signal in experiments have two contribution origins[20, 21] : one is a long-range electromagnetic (EM) effect and the other one is a short-range CT effect also called a chemical (CHEM) enhancement effect. The former is due to the localized surface plasmon resonance at the surface of metal nanoparticles, and the latter is based on a photoinduced transfer of an electron from the Fermi level of the metal to an unoccupied molecular orbital of the adsorbate (Metal → Molecule) or vice versa. It should be noted that the CT process is closely related to the coupling of the complicated metal surface, adsorbed molecules and other external sources. Until now, the CT enhancement mechanism still cannot be fully explained under certain conditions, despite the existence of the direct or indirect CT effect in some models, such as metal-semiconductor-molecule model and Au/Ag nanoparticles-molecule model *etc*.[22-28] As a consequence, we will focus on the CT enhancement mechanism when the incident light is resonant with a molecular or charge-transfer excitation of the system.

Time-dependent density functional theory (TDDFT) as a useful first-principles method has been widely-used to describe SERS enhancement mechanism, and their theoretical data can also match well with the experimental results.[25, 29-34] Moreover, pyridine molecule has become one of the most commonly used adsorbates due to its sensitive SERS-active effect.[29-32] In this work, a theoretical study of the enhanced Raman scattering of pyridine-actinides model systems is presented by employing the TDDFT method. We anticipate this study will provide a theoretical basis for future study of spectroscopy properties of actinide elements doped gold nanoparticles.

Models and Computational methods

It is common knowledge that actinide elements have distinctive optical and magnetic properties, and can present a series of electron transitions in a wide range of energy.[35] In addition, the optical and magnetism properties of actinide elements vary with their coordination environment.[36] In this case, to explore a stable SERS substrate based on actinide elements is a very challenging, important and interesting work in biomedical applications. With the development of nano-science and technology, planar structures are recently found to be a new class of nanoparticles with highly tunable optical properties, which depend on their own size and composition. These nanoparticles can be designed to either absorb or scatter light in the visible and infrared region where the penetration of light through tissue is maximal.[37-40] Based on the above considerations, a typical closed-shell planar structure is selected as SERS substrate material, Ac@Au$_7$, *i.e.* an actinium atom encapsulated in the center of Au$_7$ ring. When pyridine is adsorbed on metal surface in parallel and vertical directions respectively, the properties of seven gold atoms are equivalent due to Ac@Au$_7$ has a D$_{7h}$-like symmetry. Moreover, as a comparison, we also selected an existent Au$_8$ planer structure[41] as SERS substrate, which is the most similar model to Ac@Au$_7$ and has two different adsorption configurations as shown in Fig 1.

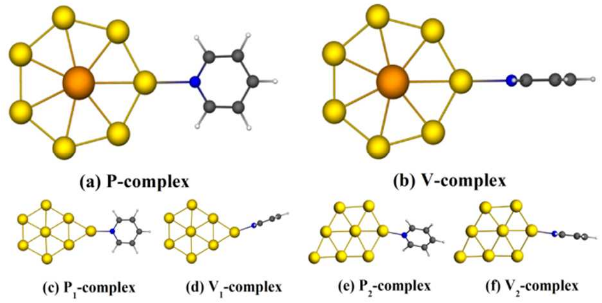

Fig. 1 Stabilized structures of six complexes. P-complex and V-complex represent two Ac@Au$_7$ planar structure with a pyridine molecule absorbed on its surface in parallel and vertical directions, respectively. The subscripts 1 and 2 represent the different adsorption sites of Au$_8$ structure. (Ac: orange, Au: luminous yellow, N: deep blue, C: deep grey, H: white)

The TDDFT method, which is based on a short-time approximation to the Raman scattering cross section, has been widely used in the theoretical study of SERS. This method not only can deal with the molecule and the metal at the same level of theory, but also can describe the different SERS enhancement mechanisms and their relation to other optical properties in a uniform way, thereby providing accurate microscopic insights into SERS. And its theoretical results for some closed-shell molecular systems are consistent with the experimental data.[42, 43]

All calculations in this study have been done by employing the Amsterdam density functional (ADF) program.[44] Considerable researches have shown that the exchange correlation functional BP86[45, 46] is appropriate for describing electronic and optical properties of metal-molecule coupled systems, whether it is pure theory or the combination of the theoretical and experimental work.[30, 33, 42, 43] And BP86 functional usually gives harmonic frequencies close to experimental results without the use of scaling factors,[47] thereby it is used in this work. Whereas we also used the statistical averaging of orbital potential (SAOP)[48, 49] to further provide more evidence for the validity of this method. The potential SAOP which displays the correct asymptotic behavior has been specially designed for calculating optical properties.[50-52] It has yielded very good results for response properties on gold dimer.[50] Relativistic corrections of heavy elements (Au, Ac) have been taken into account through zeroth order regular approximation (ZORA).[53-56] A triple-ζ with polarization functions (TZP)[57] uncontracted Slater-type orbital basis set have been used, with a [$1s^2$-$4d^{10}$] frozen core for Au and Ac, and with full electrons for N, C, and H. The geometry optimizations have been performed without imposing any symmetry constraint. All obtained structures were analyzed with vibration frequency calculations at the same level to avoid imaginary frequencies.

Absolute Raman intensities are presented as the differential Raman scattering cross-section (DRSC). For Stokes scattering with an experimental setup of a 90° scattering angle and perpendicular plan-polarized light, the cross-section is given:[58]

$$I_{Raman} = \left(\frac{d\sigma}{d\Omega}\right)_i = \frac{(2\pi)^4}{45}\frac{h}{8\pi^2 c\omega_i}\frac{(\omega_0-\omega_i)^4}{1-exp(-hc\omega_i/k_BT)}\left[45\left(\frac{d\sigma}{dQ_i}\right)^2+7\left(\frac{d\gamma}{dQ_i}\right)^2\right]$$

here, ω_0 and ω_i respectively denote the frequencies of the incident light and the ith vibrational mode; $\frac{\mathrm{d}\sigma}{\mathrm{d}Q_i}$ and $\frac{\mathrm{d}\gamma}{\mathrm{d}Q_i}$ respectively denote the derivatives of the isotropic and anisotropic polarizability of the ith vibrational mode; and h (Planck constant), c (light speed), k_B (Boltzmann constant), and T (Kelvin temperature) also respectively denote corresponding physical quantities. The finite lifetime is included phenomenologically using a damping parameter $\Gamma \approx 0.004$ a.u., which is reasonable for metal clusters and resonant Raman intensities.[29]

RESULTS and DISCUSSION

UV-visible absorption spectra

The absorption spectra of optimized complexes are obtained by TDDFT calculations in the range of ultraviolet visible (UV-vis) light, because the excitation lights are often used in SERS experiments, especially in SM-SERS detections.[3, 59-61] And the specific changes in the absorption spectra of the six complexes are shown in Supporting Information (SI) Part 1. For Ac@Au_7 planar structure, the UV-vis spectrum is principally composed of intracluster excitation (IE). However, when pyridine molecule is adsorbed on it in the form of parallel and vertical two types, in addition to intracluster transition contribution to UV-vis spectrum, the interaction between pyridine and Ac@Au_7 nanoparticle can also result in a new CT excitation transitions from the metal to the molecule. As mentioned in the introduction, the CT resonant mechanism is very important when the incident light is resonant with a molecular or CT excitation of the system. Therefore, to further understand the electron transitions behavior of the adsorption systems, we listed the typical CT excitation energies in Table 1 (the additional CT excitation energies are shown in SI Part 2). Among them, the CT excitation energy of V-complex is about 0.63 eV lower than that of P-complex, which is similar to the corresponding energy difference between surface-complex and vertex-complex for Ag_{20} cluster that is about 0.50 eV.[29] The difference of CT excited energy is easily understood if one consider the orbitals involved in the transitions. From Table 1 it is apparent that the electron transitions all from occupied MOs to thrid lowest unoccupied MO (LUMO+2), while the second highest unoccupied MO (HOMO-1) of V-complex is more active than the HOMO-5 of P-complex.

Table. 1 Calculated excitation energies (E in eV), excitation wavelengths (λ in nm), oscillator strengths (f) and orbital transitions of CT excitations for six complexes, respectively.

Geometry	E / λ	f	Transitions
P-complex	3.35 / 370	0.0058	HOMO-5 → LUMO+2
V-complex	2.72 / 456	0.0976	HOMO-1 → LUMO+2
P_1-complex	3.21 / 387	0.0231	HOMO-10 → LUMO+2
V_1-complex	2.46 / 505	0.0151	HOMO-1 → LUMO+2
P_2-complex	2.75 / 450	0.0588	HOMO-6 → LUMO+2
V_2-complex	2.78 / 446	0.0440	HOMO-5 → LUMO+2

In most cases, the intensity of resonance Raman scattering is approximately proportional to the square of oscillator strength. By comparison, we found that V-complex reveals the larger oscillator strength than any other complex, which might induce a strong resonance-enhanced Raman signal. To confirm the accuracy of CT excited energy (2.72 eV) for V-complex, we performed the calculation of absorption spectrum at SAOP/TZP level, and found that the typical CT excitation energy increased by only 0.10 eV comparing with that at BP86/TZP level. In addition, the typical IEs excitation energies are listed in SI Part 3. First, for pyridine-Ac@Au_7 complexes in Table S2, the orbitals involved in excited transitions are all from HOMOs of Ac@Au_7 to unoccupied MOs (above LUMO) of pyridine. In contrary, for the pyridine-Au_8 complexes, the electron transitions are from occupied MOs (below HOMO) of Au_8 to LUMO or LUMO+1 of pyridine. Thus, whether in the CT or IEs excited transitions, there are many obvious differences among these six complexes, although they are all formed by pyridine adsorption on gold atoms.

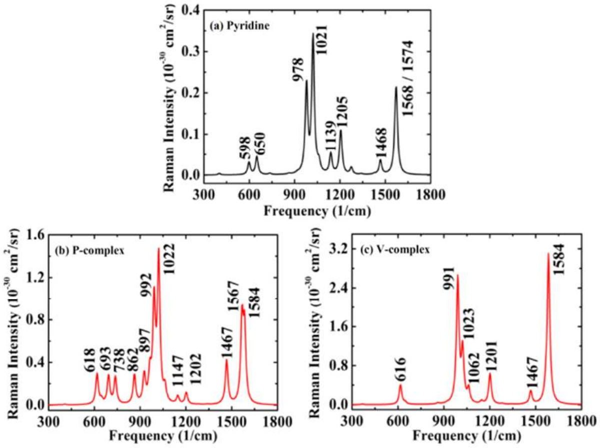

Fig. 2 Calculated static Raman spectra of Pyridine alone (a), P-complex (b), V-complex (c). Differential cross-section is measured in the unit of 10^{-30} cm^2/sr. Spectra have been broadened by a Lorentzian having a width of 20 cm^{-1}.

Enhanced Raman scattering

In order to explore how the interaction between the molecule and the metal affect the intensity of the Raman scattering, we firstly analyzed the well-known six vibrational modes of the pyridine molecule, i.e. ring deformation (598 cm^{-1}), ring breathing (978 cm^{-1} and 1021 cm^{-1}) and ring stretch vibrational modes (1205 cm^{-1}, 1468 cm^{-1}, 1568/1574 cm^{-1}), which have very obvious signals strength in SERS experiment.[3, 62] Fig 2a shows that the static DRSC is of the order of 10^{-31} cm^{2}sr^{-1} for pyridine alone, which is consistent with that of previous reported theoretical data.[30] The static Raman scattering spectra of pyridine is mainly dominated by ring breathing and stretch modes, and the relative Raman intensity of these vibrational modes is closely related to the adsorption site of pyridine. For P-complex (Fig 2b), the maximum Raman peak corresponds to ring breathing vibrational modes. Its intensity enhances by a factor of about 4 than that of pyridine alone, and several new vibration peaks appear in the SERS spectrum. For V-complex (Fig 2c), the maximum Raman peak corresponds to ring stretch vibrational mode, and its intensity increases by 16 times. The relative intensities might be attributed to sensitive to adsorption orientation of pyridine molecule. Next, for the other four complexes (see SI Part 4), their maximum Raman peaks are also correspond to ring stretch vibrational modes, and their enhancements range from 10 to 40 times. Besides the enhancement of intensity, when pyridine is adsorbed on metal surface, the typical Raman peaks will show a blue shift about 1-40 cm^{-1}. This results are consistent with the recent theoretical calculation for a pyridine adsorbed on Ag_{20} surface.[29] All these changes are induced owing to the polarization effect caused by charge redistribution of complex.

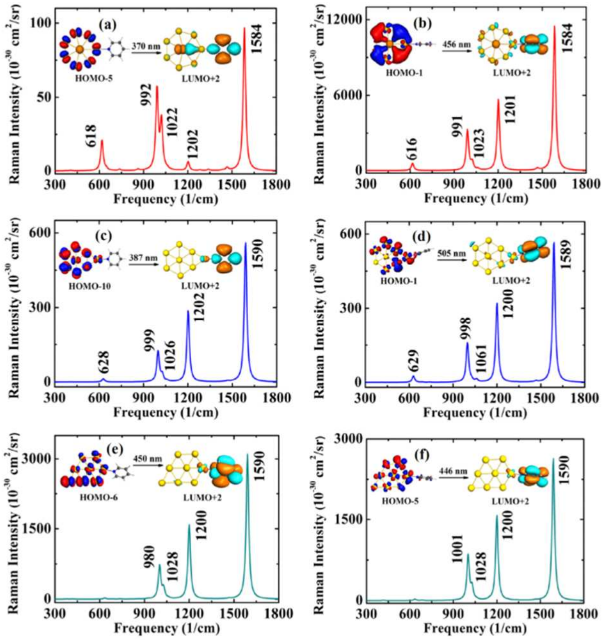

Fig. 3 Calculated CT resonance-enhanced Raman spectra for six complexes at the corresponding incident wavelength. (a) P-complex, (b) V-complex, (c) P_1-complex, (d) V_1-complex, (e) P_2-complex, (f) V_2-complex.

Next, the SERS spectra based on typical CT resonance excitations are shown in Fig 3 in the range of 300 to 1800 cm^{-1}. By comparison, we found that the CT resonance-enhanced

Raman spectra are mainly dominated by ring breathing and stretch vibrational modes, and other weaker vibrational modes (see Fig 3). This relative Raman intensity is closely related to the adsorption site of pyridine and the composition of SERS substrate materials. For P-complex, the typical absorption peaks located at 370 nm is denoted as SERS (370 nm) which is presented in Fig 3a. The Raman scattering intensity is in the order of 10^{-28} cm^2/sr, presenting an enhancement of the order of 10^3 compared to the 10^{-31} cm^2/sr of pyridine. For V-complex, the typical absorption peaks located at 456 nm is denoted as SERS (456 nm) which is shown in Fig 3b. The intensity of the order of 10^{-26} cm^2/sr corresponds to an enhancement of the order of 10^5. Next, we also simulated the CT resonance-enhanced Raman spectra for pyridine-Au@Au$_7$ complexes under their own corresponding excited light. Among them, although the CT enhancement factor is of the order of 10^4 for P$_2$-complex and V$_2$-complex, it is still 1 order of magnitude lower than that of V-complex, and these complexes are distorted seriously. In addition to list the typical CT excitation energies in main text, some additional CT excitation energies have been considered (see SI Part 2). However, due to the intensity of resonance Raman scattering is approximately proportional to the square of oscillator strength, the corresponding CT-SERS largest enhancement only can reach the order of magnitude of 10^3.

Therefore, from the above comparison, we found that the SERS enhancement intensity has a significant difference between P-complex and V-complex, even though they all have the same metal substrate. That might result from the difference of the initial orbitals involved in electron transitions. Furthermore, molecular orbital analysis shows that the SERS (456 nm) electron transitions from the 6d-5d6s (6d orbital of Ac, 5d6s hybrid orbital of Au$_7$ ring) hybrid bonding orbital to the π orbital of pyridine and slight charge transfers to the metal (HOMO-1 → LUMO+2). For other five complexes, the electrons involved in excited transitions are all from 5d or 5d6s hybrid orbitals of Au$_7$ ring. Through the above analysis, it is clear that the originate of electron transition (HOMO-1) in V-complex contain non-ignorable contribution from 6d electrons of the Ac atom. However, it is not contained in the originate in other five complexes. Therefore, the 6d electron involved in excited transitions is more likely to lead to a strong CT enhancement.

The deformation densities analysis can reveal visually photoinduced charge transfer, which has been used in SERS studies.[29, 34] From Fig 4 we can clearly see that a majority of the electron exchanges between Ac@Au$_7$ and pyridine take place in the junction of molecule-metal complexs (within black frame). However, for pyridine-Au$_8$ complexes, the electron exchange occurs in overall systems (Fig 4). Zayak *et al.* have confirmed that the intense electron exchange in interface is beneficial to chemical enhancement.[63] Therefore, Ac@Au$_7$ is more suitable to be used as SERS metal substrate material compared with pure gold system. However, for P-complex and V-complex, although they all have the same metal substrate, their Raman enhancement intensities are obviously different. To explore how the adsorption structural difference affect the Raman scattering intensity, we further analysis the process of electron exchange for P-complex and V-complex. In V-complex, the process is accomplished just in Au-N bonding region (Fig 4b). However, in P-complex, with the exception of the Au-N bonding region, we also saw enhanced electron density in the Au-H bonding region (Fig 4a). When the incident light is resonant with CT excitation of system, the electron involved in excited transition is delocalized on the molecular N-C ring, not on the H atoms. This means, the flow of electron density from the H atoms to Au atoms occurs in the Au-H bonding region, (Fig 4a, within black frame), which is enough to weaken the intensity of Au-N bonding, and then reduce the CT-SERS enhancement of P-complex. Therefore, all these facts explain why the Raman enhancement intensity of V-complex is greater than that of P-complex.

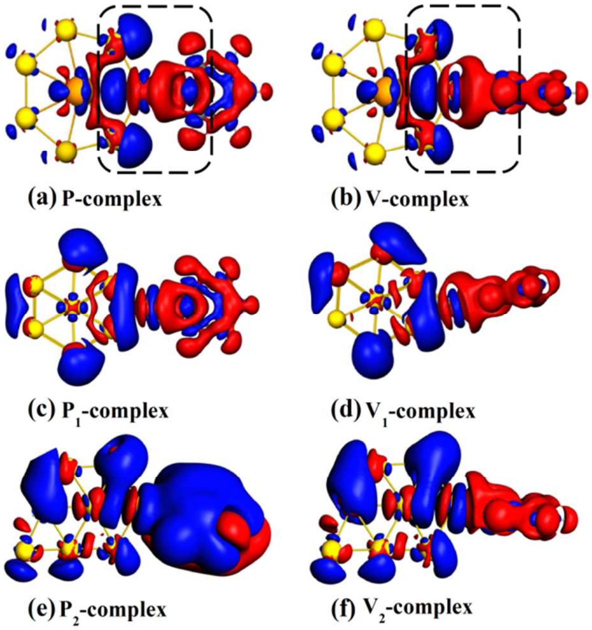

Fig. 4 Calculated deformation density ($\Delta\rho = \rho^{\mathrm{Ac@Au7+Pyridine}}$ -

$\rho^{Ac@Au7}$ - $\rho^{Pyridine}$) isosurface for the six complexes. Red and blue respectively denote an enhanced and a depleted electron density. (Isosurface value = 0.0004 a.u.)

The previous SERS experiment about actinide elements has shown that 6d electron involves in electron transitions and leads to greater intensity in the CT transition.[4] Through the above comparative analysis, the CT-SERS enhancement of V-complex is the strongest, and from Fig 3 it can be seen clearly that 6d electron of Ac atom did participate in CT excited transition of system. Inversely, although 6d electron also involved in the electron transitions in P-complex, due to pyridine molecule is adsorbed on Ac@Au$_7$ in a parallel direction, the contribution of 6d electron to excited transition is weakened. As a whole, it can be confirmed the 6d electron of actinide element induces a strong CT enhancement effect.

Table. 2 Calculated Energy decomposition analysis (kcal/mol), Au-N bond length (Å) and Voronoi deformation density (VDD)[44] charge (e) transferred for the two complexes. Values in parentheses give the percentage of each attractive term with respect to the sum of the attractive terms.

	P-complex	V-complex
$\Delta E_{electrostatic}$	-45.97 (70.51%)	-46.17 (71.34%)
ΔE_{pauli}	56.62	57.12
$\Delta E_{orbital}$	-19.23 (29.49%)	-18.55 (28.66%)
$E_{total\ binding\ energy}$	-8.58	-7.60
$E_{total\ binding\ energy}$ (BEES corrected)	-4.23	-3.94
Au-N bond length	2.43	2.42
VDD charge (molecule → metal)	0.16	0.18

$\Delta E_{electrostatic}$ is the classical electrostatic interaction term; ΔE_{pauli} is the Pauli repulsion term; $\Delta E_{orbital}$ is the orbitals interaction term. Within this energy decomposition scheme the attractive and repulsive terms are negative and positive, respectively.

Furthermore, to get a better understanding of the bonding characteristics between metal and molecule, we performed energy decomposition analysis (EDA) for P-complex and V-complex (see Table 2). Basis set superposition errors (BSSE) have been accounted for using the counterpoise method[64] by calculating the bonding energies with respect to the isolated fragments. It should be noted that, if the stabilized complex has a good symmetry, it could be seen as a typical model system. Since the conformations of pyridine-Au@Au$_7$ complexes are distorted seriously, we would not perform EDA for them. In Table 2, the Au-N bondings of the two complexes are mainly dominated by electrostatic interaction (70.51/71.34%). And despite the proportion of orbital interaction term (29.49/28.66%) in attractive term is small, it suggests an important polarization of the electron density on the surface of the cluster. The total binding energy between Ac@Au$_7$ and pyridine nicely agrees with previous reported results of another complex which is also with pyridine but adsorption on Ag$_{20}$ nanoparticles.[29] In addition, because of the increase of electron density in Au-H bonding region (see Fig 4), the total binding energy of P-complex is a little lower than that of V-complex. To quantify the charge density redistribution occurring upon pyridine bonding, atomic charges have been computed within the VDD scheme. We found that the electron exchange of V-complex is indeed more drastic than that of P-complex in Au-N bonding region, and the Au-N bond length is also shorter.

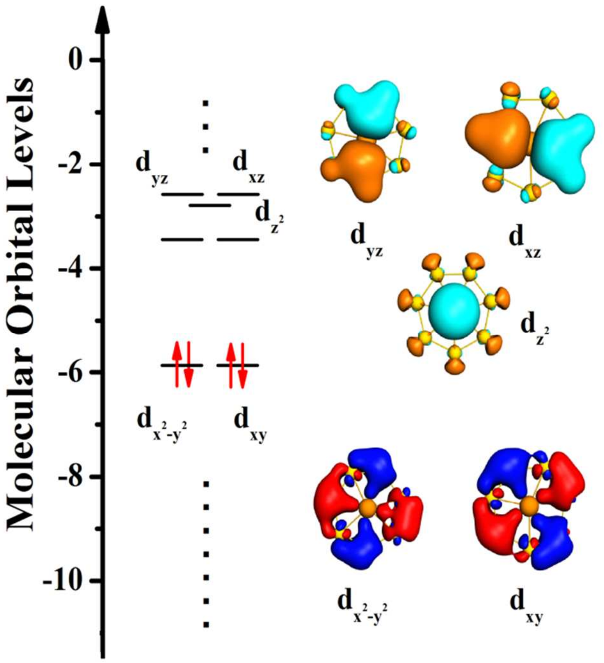

Fig. 5 Molecular orbitals (MOs) and MO energy level correlation diagram for Ac@Au$_7$ planar structure.

The binding properties of Ac@Au$_7$

In addition, to more demonstrate the reliability of our selected model, we analyzed the binding properties of Ac@Au$_7$ planar structure. The bonding in the Ac@Au$_7$ planar structure can be viewed as an Au$_7$ ring interacting with an Ac atom, which possesses a s^1, d^3 valence configuration for Au, Ac, respectively, (i.e., the 7s electrons are promoted to the 6d orbitals). The 10 valence electrons in this planar structure represent a closed-shell electronic structure (Fig 5), which is consistent with previous reported structures, such as Ti@Au$_6$, Sc@Cu$_7$.[65, 66] Among them, the two in-plane 6d orbitals (d_{xy} and d_{x2-y2}) of Ac atom play a positive role in the bonding. The average total binding energy per atom and HOMO–LUMO gap for Ac@Au$_7$ are 2.70 eV and 2.42 eV, respectively. In general, nanocluster structures with binding energy greater than 2.40 eV and HOMO–LUMO gap larger than 1.70 eV are commonly regarded to be stable.[67] Therefore, our current results suggested that Ac@Au$_7$ belongs to stable structures similar to those previously reported, such as W@Au$_{12}$, U@Au$_{14}$, Sc@Au$_{15}$ *etc*.[68-70]

Conclusions

In this work, we have researched the SERS enhancement mechanism of pyridine-Ac@Au$_7$ and pyridine-Au$_8$ model systems using TDDFT method. By calculation and comparison of the CT-SERS enhancement of these six complexes, we found that the SERS enhancement of V-complex is the strongest and can reach the order of magnitude of 10^5 at an incident wavelength of 456 nm, which could hardly be achieved in the pure gold system (about 10^3 ~ 10^4). Together with a detailed molecular orbital analysis, we surprisingly found that the initial occupied molecular orbital involved in CT excited transition in V-complex contains non-ignorable contribution from 6d electron which is not found in other five complexes. Furthermore, just as the visually deformation density isosurface shows, although the electron exchanges are drastic in Au-N bonding regions of both P-complex and V-complex, the electron exchange process occur in the Au-H bonding region is very strong enough to weaken the intensity of electron exchange of Au-N bonding. This weakening phenomenon is more specifically reflected in the charge transfer and interaction energy between the metal cluster and the molecule. Besides, the electronic structure analysis indicates that, Ac@Au$_7$ planar structure is stabilized by covalent interaction.

Spectroscopic studies of these systems that focus on molecular excited-state properties (e.g. charge-transfer states) promise a further understanding of actinide electronic structure and actinide-molecular bonding schemes. In recent years, the SERS experiment about U atom has found that the 6d orbital involved in electronic transition have greater radial extent and might lead to greater intensity in the CT transition compared with 5f orbital.[4] However, the SERS enhancement mechanism of mixed-metal substrate materials, which is consisted by actinide elements and gold nanoparticles, is still unclear. Based on a comprehensive prediction for the enhanced Raman scattering of the gold-ring structure with embedded Ac atom, we hope this study will contribute to providing a theoretical basis for the research and synthesis of new SERS substrate materials.

Acknowledgments

We would like to thank the support of the National Science Foundation of China (11374004, 11034003) and the Science and Technology Development Program of Jilin Province of China (20150519021JH). Z. W. also acknowledges the assistance of the Fok Ying Tung Education Foundation (142001) and the High Performance Computing Center (HPCC) of Jilin University.

Notes and references

[a] *Institute of Atomic and Molecular Physics, Jilin University, Changchun, 130012, China*
[b] *Jilin Provincial Key Laboratory of Applied Atomic and Molecular Spectroscopy (Jilin University), Changchun, 130012, China.*
[c] *Key Laboratory for Molecular Enzymology and Engineering of Ministry of Education, College of Life Sciences, Jilin University, Changchun, 130012, China.*

E-mail: wangzg@jlu.edu.cn

† Electronic Supplementary Information (ESI) available: [The IEs of pyridine-Ac@Au$_7$ and pyridine-Au$_8$ complexes. Calculated static Raman spectra of pyridine-Au$_8$ complexes]. See DOI: 10.1039/b000000x/

1. L. Jensen, C. M. Aikens and G. C. Schatz, *Chem. Soc. Rev*, 2008, **37**, 1061-1073.
2. D. Y. Wu, J. F. Li, B. Ren and Z. Q. Tian, *Chem. Soc. Rev*, 2008, **37**, 1025-1041.
3. Z. Q. Tian, B. Ren and D. Y. Wu, *J. Phys. Chem. B*, 2002, **106**, 9463-9483.
4. R. E. D. Re, K. C. Jantunen, J. T. Golden, J. L. Kiplinger and D. E. Morris, *J. Am. Chem. Soc.*, 2005, **127**, 682-689.
5. R. Olivares-Amaya, D. Rappoport, P. A. Munoz, P. Peng, E. Mazur and A. Aspuru-Guzik, *J. Phys. Chem. C*, 2012, **116**, 15568-15575.
6. P. P. Patra and G. V. P. Kumar, *J. Phys. Chem. Lett*, 2013, **4**, 1167-1171.
7. A. Sivanesan, E. Witkowska, W. Adamkiewicz, L. Dziewit, A. Kaminska and J. Waluk, *The Analyst*, 2014, **139**, 1037-1043.
8. J. Suntivich, Z. Xu, C. E. Carlton, J. Kim, B. Han, S. W. Lee, N. Bonnet, N. Marzari, L. F. Allard, H. A. Gasteiger, K. Hamad-Schifferli and Y. Shao-Horn, *J. Am. Chem. Soc.*, 2013, **135**, 7985-7991.
9. Y. Wang, L. Chen and P. Liu, *Chem. Eur. J*, 2012, **18**, 5935-5943.

10. Y. Yin, T. Qiu, L. Ma, X. Lang, Y. Zhang, G. Huang, Y. Mei and O. G. Schmidt, *J. Phys. Chem. C*, 2013, **116**, 25504-25508.
11. Y. Zhou, C. Lee, J. Zhang and P. Zhang, *J. Mater. Chem. C*, 2013, **1**, 3695–3699.
12. L. Chen, Z. Li, Y. Meng, M. Lu, Z. Wang and R. Q. Zhang, *J. Phys. Chem. C*, 2013, **117**, 12544-12551.
13. L. Chen, Y. Gao, H. Xu, Z. Wang, Z. Li and R. Q. Zhang, *Phys. Chem. Chem. Phys*, 2014, **16**, 20665-20671.
14. S. Schlucker, *Angew. Chem. Int. Edit.*, 2014, **53**, 4756-4795.
15. G. Henriksen, O. S. Bruland and R. H. Larsen, *Anticancer. Res*, 2004, **24**, 101-106.
16. S. N. Nahar, A. K. Pradhan and S. Lim, *Can. J. Phys*, 2011, **89**, 483-494.
17. S. G. Kang, G. Zhou, P. Yang, Y. Liu, B. Sun, T. Huynh, H. Meng, L. Zhao, G. Xing, C. Chen, Y. Zhao and R. Zhou, *P. Natl. Acad. Sci. USA*, 2012, **109**, 15431-15436.
18. S. G. Kang, T. Huynh and R. Zhou, *Nanoscale*, 2013, **5**, 2703-2712.
19. S. G. Kang, T. Huynh and R. Zhou, *Sci. Rep*, 2012, **2**, 957.
20. H. Xu, E. J. Bjerneld, M. Käll and L. Börjesson, *Phys. Rev. Lett*, 1999, **83**, 4357.
21. M. Moskovits, *Rev. Mod. Phys.*, 1985, **57**, 783-826.
22. B. Nikoobakht, J. Wang and M. A. El-Sayed, *Chem. Phys. Lett*, 2002, **366**, 17-23.
23. E. Hao and G. C. Schatz, *J. Chem. Phys*, 2004, **120**, 357-366.
24. D. P. Fromm, A. Sundaramurthy, P. J. Schuck, G. Kino and W. E. Moerner, *Nano. Lett*, 2004, **4**, 957-961.
25. L. Zhao, L. Jensen and G. C. Schatz, *Nano. Lett*, 2006, **6**, 1229-1234.
26. Z. Sun, C. Wang, J. Yang, B. Zhao and J. R. Lombardi, *J. Phys. Chem. C*, 2008, **112**, 6093-6098.
27. L. Peyser-Capadona, J. Zheng, J. I. Gonzalez, T. H. Lee, S. A. Patel and R. M. Dickson, *Phy. Rev. Lett*, 2005, **94**, 058301.
28. C. H. Xiao, B. X. Xiao, Y. D. Wang, J. Zhang, S. M. Wang, P. Wang, T. Yang, R. Zhao, H. Yu., Z. F. Li and M. Z. Zhang, *RSC Advances*, 2015, **5**, 17945-17952.
29. L. Zhao, L. Jensen and G. C. Schalz, *J. Am. Chem. Soc*, 2006, **128**, 2911-2919.
30. L. Jensen, L. L. Zhao and G. C. Schatz, *J. Phys. Chem. C*, 2007, **111**, 4756-4764.
31. D. Y. Wu, M. Hayashi, C. H. Chang, K. K. Liang and S. H. Lin, *J. Chem. Phys*, 2003, **118**, 4073.
32. D. Y. Wu, M. Hayashi, S. H. Lin and Z. Q. Tian, *Spectrochim. Acta, Part A*, 2004, **60**, 137-146.
33. N. Valley, N. Greeneltch, R. P. Van Duyne and G. C. Schatz, *J. Phys. Chem. Lett*, 2013, **4**, 2599-2604.
34. L. Xia, M. Chen, X. Zhao, Z. Zhang, J. Xia, H. Xu and M. Sun, *J. Raman. Spectrosc*, 2014, **45**, 533-540.
35. J. J. Katz, G. T. Seaborg and L. R. Morss, *Chapman and Hall : New York*, 1986.
36. G. Tian, J. Xu and L. Rao, *Angewandte Chemie*, 2005, **117**, 6356-6359.
37. L. R. Hirsch, A. M. Gobin, A. R. Lowery, F. Tam, R. A. Drezek, N. J. Halas and J. L. West, *Ann. Biomed. Eng*, 2006, **34**, 15-22.
38. Z. Li, Z. Liu, J. Zhang, B. Han, J. Du, Y. Gao and T. Jiang, *J. Phys. Chem. B*, 2005, **109**, 14445-14448.
39. C. Zhu, G. Meng, Q. Huang, Z. Zhang, Q. Xu, G. Liu, Z. Huang and Z. Chu, *Chem. Commun*, 2011, **47**, 2709-2711.
40. P. Xu, B. Zhang, N. H. Mack, S. K. Doorn, X. Han and H.-L. Wang, *J. mater. Chem*, 2010, **20**, 7222-7226.
41. H. Hakkinen, B. Yoon, U. Landman, X. Li, H. Zhai and L.-S. Wang, *J. Phys. Chem. A*, 2003, **107**, 6168-6175.
42. A. Mohammed, W. Hu, P. O. Andersson, M. Lundquist, L. Landström, Y. Luo and H. Ågren, *Chem. Phys. Lett*, 2013, **581**, 70-73.
43. X. Zhao and M. Chen, *J. Raman. Spectrosc*, 2014, **45**, 62-67.
44. G. Te Velde, F. M. Bickelhaupt, E. J. Baerends, C. Fonseca Guerra, S. J. A. Van Gisbergen, J. G. Snijders and T. Ziegler, *J. Comput. Chem*, 2001, **22**, 931-967.
45. A. D. Becke, *Phys. Rev. A*, 1988, **38**, 3098-3100.
46. J. Perdew, *Phy. Rev. B*, 1986, **33**, 8822-8824.
47. J. Neugebauer and B. A. Hess, *J. Chem. Phys*, 2003, **118**, 7215-7225.
48. O. V. Gritsenko, P. R. T. Schipper and E. J. Baerends, *Chem. Phys. Lett*, 1999, **302**, 199-207.
49. P. R. T. Schipper, O. V. Gritsenko, S. J. A. van Gisbergen and E. J. Baerends, *J. Chem. Phys*, 2000, **112**, 1344.
50. K. R. Geethalakshmi, F. Ruiperez, S. Knecht, J. M. Ugalde, M. D. Morse and I. Infante, *Phys. Chem. Chem. Phys*, 2012, **14**, 8732-8741.
51. F. Rabilloud, *J. Chem. Phys*, 2014, **141**, 144302.
52. B. Anak, M. Bencharif and F. Rabilloud, *RSC Advances*, 2014, **4**, 13001.
53. E. v. Lenthe, A. Ehlers and E. J. Baerends, *J. Chem. Phys.*, 1999, **110**, 8943.
54. E. v. Lenthe, E. J. Baerends and J. G. Snijders, *J. Chem. Phys.*, 1993, **99**, 4597-4610.
55. E. v. Lenthe, J. G. Snijders and E. J. Baerends, *J. Chem. Phys.*, 1996, **105**, 6505-6516.
56. E. v. Lenthe, E. J. Baerends and J. G. Snijders, *J. Chem. Phys.*, 1994, **101**, 9783-9792.
57. E. v. Lenthe and E. J. Baerends, *J. Comput. Chem.*, 2003, **24**, 1142-1156.
58. J. Neugebauer, M. Reiher, C. Kind and B. A. Hess, *J. Comput. Chem*, 2002, **23**, 895-910.
59. M. G. Albrecht and J. A. Creighton, *J. Am. Chem. Soc*, 1977, **99**, 5215-5217.
60. P. R. Carey, *J. Biol. Chem*, 1999, **274**, 26625-26628.
61. M. Moskovits, *J. Raman. Spectrosc*, 2005, **36**, 485-496.
62. D. Y. Wu, X. M. Liu, S. Duan, X. Xu, B. Bin, S. H. Lin and Z. Q. Tian, *J. Phys. Chem. C.*, 2008, **112**, 4195-4204.
63. A. T. Zayak, Y. S. Hu, H. Choo, J. Bokor, S. Cabrini, P. J. Schuck and J. B. Neaton, *Phys. Rev. Lett.*, 2011, **106**, 083003.
64. S. F. Boys and F. Bernardi, *Mol. Phys*, 1970, **19**, 553-566.
65. X. Li, B. Kiran, L.-F. Cui and L.-S. Wang, *Phys. Rev. Lett*, 2005, **95**, 253401.
66. T. Holtzl, E. Janssens, N. Veldeman, T. Veszpremi, P. Lievens and M. T. Nguyen, *Chem. Phys. Chem.*, 2008, **9**, 833-838.

67. Y. Gao, S. Bulusu and X. C. Zeng, *Chem. Phys. Chem.*, 2006, **7**, 2275-2278.

68. P. Pyykko and N. Runeberg, *Angew. Chem. Int. Edit.*, 2002, **114**, 2278-2280.

69. Y. Gao, S. Bulusu and X. C. Zeng, *J. Am. Chem. Soc.*, 2005, **127**, 15680-15681.

70. Y. Gao, X. Dai, S. G. Kang, C. A. Jimenez-Cruz, M. Xin, Y. Meng, J. Han, Z. Wang and R. Zhou, *Sci. Rep.*, 2014, **4**, 5862.

TOC

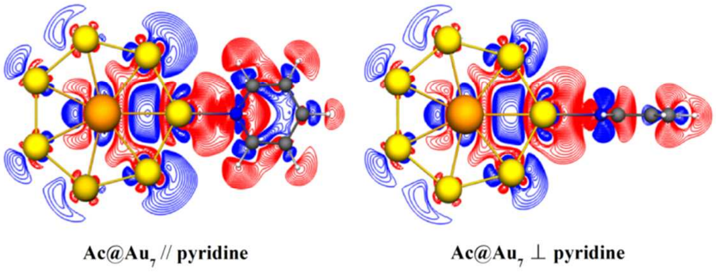

The 6d electrons of Ac atom involved in excited transitions induce a strong CT-SERS enhancement which can be tuned by changing the conformation of pyridine-Ac@Au$_7$ complexes.